

pubs.acs.org/JPCA Article

# Proton Transfer in Phosphoric Acid-Based Protic Ionic Liquids: Effects of the Base

Zhenghao Zhu, Xubo Luo, Alexei P. Sokolov, and Stephen J. Paddison\*



Cite This: J. Phys. Chem. A 2020, 124, 4141-4149



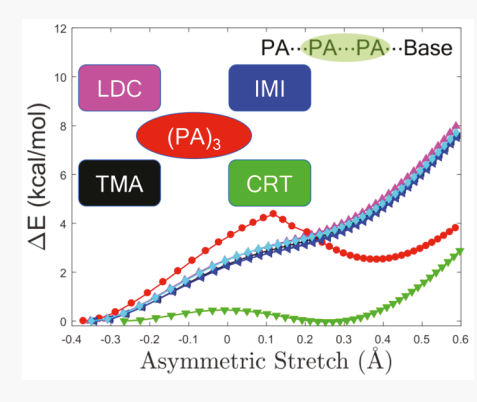
**ACCESS** 

Metrics & More

Article Recommendations

Supporting Information

**ABSTRACT:** Electronic structure calculations were performed to understand highly decoupled conductivities recently reported in protic ionic liquids (PILs). To develop a molecular-level understanding of the mechanisms of proton conductivity in PILs, minimum-energy structures of trimethylamine, imidazole, lidocaine, and creatinine (CRT) with the addition of one to three phosphoric acid (PA) molecules were determined at the B3LYP/6-311G\*\* level of theory with the inclusion of an implicit solvation model (SMD with  $\varepsilon=61$ ). The proton affinity of the bases and zero-point energy corrected binding energies were computed at a similar level of theory. Proton dissociation from PA occurs in all systems, resulting in the formation of ion pairs due to the relatively strong basicity of the bases (proton acceptors) and the effect of the high dielectric constant solvent in stabilizing the charge separation. The second and third PA molecules preferentially form "ring-like" hydrogen bonds with one another instead of forming hydrogen bonds at the donor and acceptor sites of the bases. Potential energy scans reveal that the bases with stronger proton affinity exert greater



influence on the energetics of proton transfer between the individual PA molecules. However, the effects are minimal when shifted into a single-well from a double-well potential. Barrierless proton transfer was observed to occur in the CRT system with several PA molecules present, implying that the CRT may be a promising PA-based PIL.

# **■ INTRODUCTION**

Ionic liquids may be aprotic, zwitterionic, or protic in their chemical compositions. Protic ionic liquids (PILs) are typically the combinations of Brønsted-Lowry acids and bases. Their promising properties, including high thermal and electrochemical stability, low vapor pressure, and high open circuit voltage and efficiency, have driven PILs to become favorable anhydrous electrolytes used in the fuel cells.<sup>2,3</sup> Thus, PILs have attracted significant attention for the investigation of their perspective properties and potential use in various applications.<sup>2–4</sup> Recent studies<sup>5,6</sup> revealed exceptionally strong decoupling of proton conductivity from viscosity in a mixture of lidocaine (LDC) with phosphoric acid (PA). Proton conductivity in this mixture even exceeds that of PA at a similar viscosity. Both LDC and PA possess proton donor and acceptor sites, which is deemed to be of central importance to build up hydrogen bond networks with an efficient proton transport mechanism. For comparison, trimethylammonium has only one proton acceptor site, and its mixture with H<sub>2</sub>PO<sub>4</sub><sup>-</sup> has significantly lower conductivity than LDC with PA at the same viscosity.6 Hence, it is necessary to develop a fundamental molecular-level understanding of the chemical and structural aspects that control proton transfer in these PILs.

The two main types of proton transport mechanisms are (1) vehicular in which a molecular entity "carries" the excess positive charge and (2) structural diffusion where protons

move by being transferred through the connected hydrogen bond network with a change of the proton identity. <sup>7–12</sup> The high efficiency of the latter is generally viewed to be the principal reason for the high proton conductivity in neat PA and high diffusivity in slightly acidic water. 13-18 Generally, it is expected that the chemical structure and orientation of the Brønsted-Lowry acid-base pair is responsible for the formation of hydrogen bond networks that facilitates fast proton diffusivity in a PIL. 9,19 Several experimental investigations have been performed to elucidate the mechanisms of proton transport in PILs. Hoarfrost and co-workers<sup>20</sup> found that the proton conductivity was enhanced by the proton hopping as well as the long-range transport in the PIL imidazolium bis(trifluoromethylsulfonyl)imide through pulsedfield gradient NMR and quasi-elastic neutron scattering techniques. Kreuer et al.<sup>21</sup> compared the experimentally measured self-diffusion coefficient of proton with that obtained by using the Nernst-Einstein relation in three imidazole (IMI)-doped systems. They attributed the greatest contribu-

Received: March 31, 2020 Revised: April 20, 2020 Published: April 21, 2020





tion to structural diffusion of the proton. It is impossible to have a fundamental molecular-level understanding of the chemical and structure aspects that control the proton conductivity in PILs from only experimental studies.

Quantum mechanical calculations have been successfully performed to study the mechanisms of proton transfer in many different systems. 8,10,11,22-29 For example, Scheiner and Yi<sup>30-36</sup> systematically investigated the effects of external ions and molecular charge and methyl substitution as well as stretches and bends of the hydrogen bond on energetics for proton transfer in a number of different systems. In the work of Clark et al., 26 three pairs of ionomers (fully fluorinated sulfonyl imides, partially fluorinated sulfonyl imides, and aromatic sulfonic acid-based materials) were investigated to compare the role of the neighboring group substitutions on the proton dissociation of hydrated acidic moieties. Wang and Paddison<sup>3</sup> examined the hydrogen bonding and energetics related to proton transport of substituted phosphonic acid molecules and their self-condensation products and found that the fluorinated molecules show stronger binding to water than the nonfluorinated molecules. Recently, Sepehr and Paddison<sup>22,23</sup> investigated the effects of sulfuric and triflic acids on the hydration of vanadium species within a highly acidic environment and studied the primary hydration and proton transfer of 10 acid molecules including CF<sub>3</sub>SO<sub>3</sub>H, FSO<sub>3</sub>H, CH<sub>3</sub>SO<sub>3</sub>H, H<sub>2</sub>SO<sub>4</sub>, and so forth. Kumar and Venkatnathan studied the mechanism of proton transport in several systems including ionic liquid-doped perfluorosulfonic acid memimidazolium methanesulfonate ionic liquid,<sup>39</sup> and IMI chains.<sup>40</sup> Additionally, ab initio molecular dynamics (AIMD) simulations have been extensively applied into various systems 9,10,14-16,41 and provided insightful interpretation of the proton-transfer mechanisms.

The present work focuses on the influence of the chemical composition and molecular geometry of several bases on proton dissociation and transfer in the PA-based PILs. These results will form the basis for simulations of extended systems using AIMD. Specially, in the reported studies here, quantum chemical calculations were performed on systems of PA paired with trimethylamine (TMA), IMI, LDC, and creatinine (CRT). The computational details are briefly described in the following section followed by the results and discussion. Finally, the major findings are concluded in the last section.

#### COMPUTATIONAL DETAILS

We carried out all electronic structure calculations with the GAUSSIAN 09 suite of programs. 42 The molecular geometry optimizations of bases and acids were initially performed with Hartree-Fock theory and the 6-31G\*\* split valence basis set<sup>43,44</sup> with conjugate gradient methods<sup>45</sup> without symmetry constraints. Hybrid density functional theory with Beck's 3 parameter functional (B3LYP)<sup>46-49</sup> using the same basis set was employed to further optimize electronic structures, followed by the final refinement of structures at the B3LYP/ 6-311G\*\* level. 50 This procedure was found to be the most efficient approach for obtaining the fully optimized global minimum-energy structure. The effect of the dispersion interactions has been tested in previous work<sup>25</sup> by comparing the results of the B3LYP functional to the dispersion-corrected B97D functional,<sup>51</sup> and only minor differences in the optimized structures and energetics for proton transfer were observed. Subsequently, the density-based solvation model (SMD)<sup>52</sup> was implemented to all the optimized structures

considering the effect of the environment of PA (at a high dielectric constant,  $\varepsilon=61)^{53}$  on the global minimum-energy structures and proton transfer. It is worth emphasizing that there is a minimal effect of the numerical value of the dielectric constant on the energetics for the proton transfer (see Figure S1). The choice of B3LYP/6-311G\*\* with the SMD model is due to its success and reliability when applying into many systems previously. The calculation of frequency at the same level of theory were undertaken to confirm local minima without imaginary frequency and zero-point energies (ZPEs) for each of the systems. Proton affinities of bases and molecular binding energies of PA molecules to different bases were calculated from the ZPE-corrected total electronic energies.

In the present study, from 1 to 3 PA molecules were added to the fully optimized structures of each base starting from different initial positions. We selected the lowest energy structure for each system as the "ground state" structure. The potential energy surface (PES) scan at the B3LYP/6-311G\*\*/ SMD level of theory was employed on the optimized structures of pairs and clusters of the PA molecules with the bases to determine the relative energetics (i.e., energetic barrier) associated with proton transfer from a proton donor to an acceptor site. The profiles of the energy associated with the proton transfer were obtained by incrementally changing the length of the OH or NH between the transferring proton and the oxygen or nitrogen accepting the proton with steps of 0.02 Å where this bond length is the only fixed parameter and the optimization was carried out over all other degrees of freedom without symmetry constraints at each step of the scan. A reverse set of scans was also implemented by decreasing the bond length of the OH or NH in the same step starting from the geometry obtained at the last step of the original scan. The energetic profiles were plotted via selecting the configuration with the lower energy at the same OH or NH bond length from the forward and the reverse scans. A transition state (TS) structure was further optimized via the Berny algorithm and confirmed by the determination of one imaginary frequency.

# ■ RESULTS AND DISCUSSION

Optimized Structures of Base + nPA (n = 1-3). The fully optimized configurations of one PA molecule paired with (a) TMA; (b) IMI; (c) LDC; and (d) CRT were obtained, and the minimum energy structures at the B3LYP/6-311G\*\* level with inclusion of the implicit solvation effect are illustrated in Figure 1. The hydrogen bond lengths between the molecules (i.e., the O···O or O···N separation) are denoted by double arrow lines along with the corresponding lengths in Å because this is an important feature of proton transfer in PILs. The proton affinity is an important parameter indicating the entity's capability of intrinsically attracting a proton. Computed affinities in the gas phase and with the continuum solvation model are reported in Table 1. The results demonstrate that the inclusion of an implicit solvent noticeably raises the proton affinity of the four investigated bases to various extents as the positively charged base molecules are stabilized by the high dielectric constant solvent. Comparison with the experimental values of TMA and IMI in the gas phase shows that our computed affinities are in good agreement at the B3LYP/6-311G\*\* level of theory. The order of the proton affinities calculated with the SMD model is as follows: LDC > TMA > CRT > IMI. Generally, the proton dissociation from PA occurs in four systems, resulting in the formation of ion

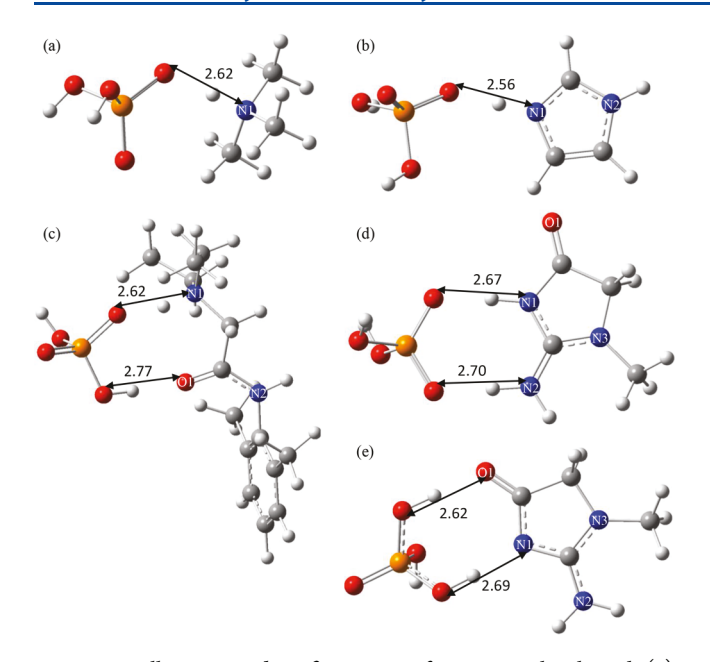


Figure 1. Fully optimized configurations of one PA molecule with (a) TMA, (b) IMI, (c) LDC, (d) CRT, and (e) CRT\* (congener of CRT cluster) at the B3LYP/6-311G\*\*/SMD level of theory. All values are reported in Å. The atomic color schemes in Figures 1 and 2 are hydrogen (white), carbon (gray), nitrogen (blue), oxygen (red), and phosphor (orange). Although there is one more hydrogen bond between O1 and PA in system LDC + 1PA, the distances between O···N1 in both TMA + 1PA system and LDC + 1PA system are the same. In the CRT + 1PA system, there are two hydrogen bonds, while the N2···PA hydrogen bond is formed between the acceptor site of the PA molecule and the donor site of the CRT compared to the O1···PA hydrogen bond built between the donor site of PA and the acceptor site of the LDC. CRT\* + 1PA is less energetic favorable than the structure of CRT + 1PA by 1.1 kcal/mol.

Table 1. Proton Affinities for the Bases

	proton affinities/kcal mol <sup>-1</sup>			
	gas phase <sup>a</sup>	$SMD^{b}$	Exp.	
TMA	226.12	289.36	231.44 <sup>c</sup>	
IMI	227.46	283.97	229.95 <sup>c</sup>	
LDC (N1 site)	240.85	290.15		
LDC (O1 site)	222.45	264.11		
CRT (N1 site)	234.47	286.04		
CRT (O1 site)	230.63	273.09		

<sup>a</sup>ZPE-corrected proton affinities at the B3LYP/6-311G\*\* level of theory in the gas phase. <sup>b</sup>ZPE-corrected proton affinities at the B3LYP/6-311G\*\* level of theory with the SMD model. <sup>c</sup>From ref 57.

pairs consisting of the positively charged base and negatively charged anion  ${\rm H_2PO_4}^-$  due to the relatively strong basicity of the bases and the effect of the high dielectric constant solvent on stabilizing the charge separation. In Figure 1a, there is only one hydrogen bond of 2.62 Å in the open structure of TMA + 1PA as the TMA molecule possesses only one proton accepting site. Although IMI has both proton donor and acceptor sites, only one hydrogen bond of 2.56 Å exists in the system of IMI + 1PA shown in Figure 1b because of the coplanar heterocycle of the IMI molecule. In Figure 1c,d, the equilibrium structures show that the PA molecule adopts a similar orientation paired with LDC and CRT leading to a "ring-like" hydrogen bonding network, though these two bases have different geometries. The critical differences in their

configurations are that the PA molecule in the CRT + 1PA cluster acts as both a hydrogen bond donor and acceptor with two hydrogen bonds of intermediate length (2.67 and 2.70 Å) while the PA molecule in the LDC + 1PA system plays the role of an hydrogen bond donor forming a short hydrogen bond of 2.62 Å and a weak hydrogen bond of 2.77 Å, demonstrating the characteristics of PA molecules: three proton donor sites and one proton acceptor site contributing to the configurational frustration in pure PA. 15 It is worth noting that there is a congener of CRT\* + 1PA (distinguished by \*) shown in Figure 1e. In this case, two hydrogen bonds were formed with O1 and N1 of the CRT molecule instead of N1 and N2 atoms in the CRT + 1PA pair, showing similar hydrogen bond networks with the LDC + 1PA system, except that the proton is still associated with PA in CRT\* + 1PA due to the interaction between O1 and N1 of the CRT molecule. This geometric isomer is less favorable in energy by 1.1 kcal/mol.

The fully optimized structures of TMA, IMI, LDC, CRT, and CRT\* with the addition of two PA molecules are shown in Figure S2. There is little difference in the hydrogen bonding networks between the bases and PA molecules except for the observed increase in hydrogen bond length. It was noted that the second PA molecule preferentially forms "ring-like" hydrogen bonds ranging from 2.50 to 2.73 Å with the first PA molecule rather than with available hydrogen bond donor and acceptor sites of the base (based on the minimum energy structure at the B3LYP/6-311G\*\*/SMD level of theory), as were the cases for the complexes of bases with subsequently adding the third PA molecule (see Figure 2); the hydrogen bond lengths continuously increase to some extent, resulting in slight shortening of the covalent bond between the dissociated

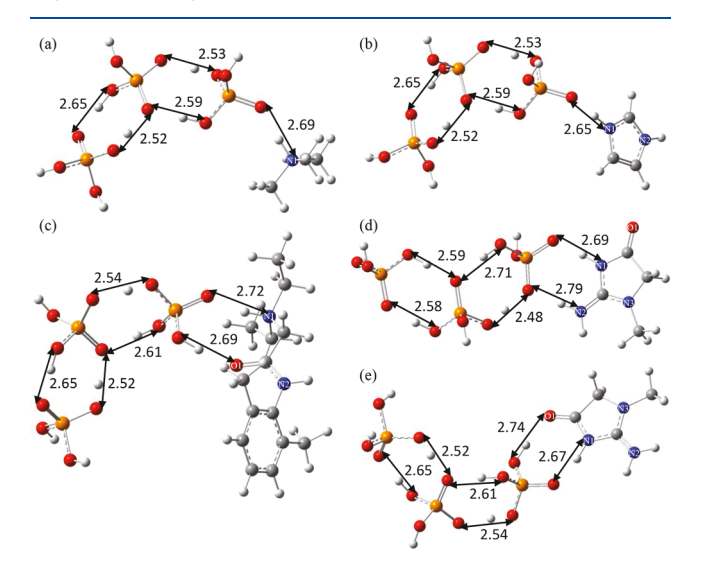


Figure 2. Fully optimized configurations of cluster of three PA molecules with (a) TMA, (b) IMI, (c) LDC, (d) CRT, and (e) CRT\* (congener of CRT cluster) at the B3LYP/6-311G\*\*/SMD level of theory. All values are reported in Å. The second and third PA molecules energetic preferentially form "ring-like" hydrogen bonds ranging from 2.48 to 2.73 Å with the PA molecule rather than with available hydrogen bond donor and acceptor sites of the base. Compared with systems of base + 1PA, the hydrogen bond distances between N1 and PA in all systems increase to various extents (the most for IMI and LDC systems), while the structures of the clusters of PA molecules formed through hydrogen bonding are similar. CRT\* + 3PA is more energetic favorable than the structure of CRT + 3PA by 1.1 kcal/mol.

Table 2. Structural Parameters of PA-Based PILs at the Level of B3LYP/6-311G\*\*/SMD

	r(N1···O)	r(N2/O1···O)	$r(O\cdots O)(1st \text{ and } 2nd PA)$		$r(O\cdots O)(2nd \text{ and } 3rd PA)$	
TMA-1PA	$2.62 (1.07)^b$					
IMI-1PA	2.56 (1.09)					
LDC-1PA	2.62 (1.08)	2.77 (0.98)				
CRT-1PA	2.67 (1.06)	2.70 (1.05)				
CRT*-1PA	2.69 (1.01)	2.62 (1.01)				
TMA-2PA	2.68 (1.05)		2.51 (1.04)	2.53 (1.03)		
IMI-2PA	2.63 (1.06)		2.54 (1.02)	2.73 (0.99)		
LDC-2PA	2.71 (1.06)	2.69 (0.98)	2.54 (1.02)	2.55 (1.02)		
CRT-2PA	2.68 (1.05)	2.78 (1.04)	2.50 (1.04)	2.66 (0.99)		
CRT*-2PA	2.66 (1.06)	2.75 (0.98)	2.54 (1.03)	2.55 (1.02)		
TMA-3PA	2.69 (1.05)		2.53 (1.02)	2.59 (1.01)	2.52 (1.03)	2.65 (0.99)
IMI-3PA	2.65 (1.05)		2.53 (1.02)	2.59 (1.01)	2.52 (1.03)	2.65 (0.99)
LDC-3PA	2.72 (1.05)	2.69 (0.98)	2.54 (1.02)	2.61 (1.01)	2.52 (1.03)	2.65 (0.99)
CRT-3PA	2.69 (1.05)	2.79 (1.03)	2.48 (1.05)	2.63 (0.99)	2.58 (1.01)	2.59 (1.01)
CRT*-3PA	2.67 (1.05)	2.74 (0.99)	2.54 (1.02)	2.61 (1.01)	2.52 (1.03)	2.65 (0.99)

<sup>&</sup>quot;All reported values are in the unit of Å. "Values in parenthesis are the distances of covalent bond N-H or O-H.

H atom and protonated N1 atom of the bases from various distances to the same final value of 1.05 Å (see Table 2). It is interesting to note that the distances of the hydrogen bonds formed between the second and third PA molecules are the same (2.65 and 2.52 Å) for all of the base + 3PA systems (shown in Figure 2a-c,e) except for the CRT + 3PA complex in Figure 2d with two comparable hydrogen bonds (2.58 and 2.59 Å), which implies that the hydrogen bonding networks between the second and third PA molecules are influenced by the base molecules even separated by another PA molecule. In most of the studied systems, the charged ions were separated by a neutral PA molecule forming the complex: base-H+... PA···PA<sup>-</sup>···PA, in which the excess charge is delocalized over the PA molecules through the hydrogen bonding network. Specifically, the contact ion pairs were only observed in the system of CRT + 3PA (see Figure 2d) in the form of CRT-H+...PA-...PA because the original proton accepting oxygen of a PA in the proximity of CRTH+ not only forms a hydrogen bond with the N2 atom of the CRT molecule but also with the neighboring PA molecule.

Examination of the ZPE-corrected binding energies of the PA molecules to the various bases (shown in Table 3) indicates that the first PA molecule is most loosely bound to IMI in comparison with the other systems, while the binding energy per PA molecule increases with the addition of more PA molecules because the second and third PA molecules form double hydrogen bonds with the first PA. Although only one hydrogen bond is formed in the TMA + 1PA complex, a much larger ZPE-corrected binding energy of 18.26 kcal/mol is observed, meaning that the basicity of TMA is stronger than IMI, which is confirmed by the greater proton affinity of TMA (see Table 1). It is also noted that the ZP-corrected binding energies of PA to LDC increase followed by the slight decrease with adding PA molecules, which implies that the PA molecule is more strongly bound to another PA molecule than to LDC. Similar magnitude in the binding energy per PA is observed in both systems of CRT + nPA and CRT\* + nPA (n = 1-3), revealing that there is a small difference in binding energies between the PA molecules and PA and CRT. It is important to recognize that the shorter the hydrogen bond, the stronger the binding energy when there is no accompanying covalent bond breaking and formation. However, the equilibrium structures show that the proton initially covalently bonded to PA has

Table 3. Energetics of PA-Based PILs at the Level of B3LYP/6-311G\*\*/SMD

	$E_{\rm elec} + \rm ZPE^a$	$\Delta E_{\rm ZPE}^{b}/{\rm kcal\ mol^{-1}}$	$\Delta E^c/\text{kcal mol}^{-1}$
PA	-644.239902		
TMA	-174.413899		
LDC	-731.370596		
IMI	-226.229286		
CRT	-396.153573		
TMA-1PA	-818.682904	-18.26	-18.26
IMI-1PA	-870.491277	-13.86	-13.86
LDC-1PA	-1375.639985	-18.50	-18.50
CRT-1PA	-1040.427675	-21.46	-21.46
CRT*-1PA	-1040.425845	-20.31	-20.31
TMA-2PA	-1462.960320	-41.80	-20.90
IMI-2PA	-1514.765266	-35.26	-17.63
LDC-2PA	-2019.919933	-43.64	-21.82
CRT-2PA	-1684.699093	-41.24	-20.62
CRT*-2PA	-1684.699342	-41.39	-20.69
TMA-3PA	-2107.229423	-60.12	-20.04
IMI-3PA	-2159.036694	-55.02	-18.34
LDC-3PA	-2664.189472	-62.22	-20.74
CRT-3PA	-2328.966906	-58.74	-19.58
CRT*-3PA	-2328.968909	-60.01	-20.00

<sup>a</sup>Total electronic energy corrected for ZPE in Hartrees. <sup>b</sup>Energy difference based on ZPE-corrected electronic energies (*i.e.*  $\Delta E_b = E[\mathbf{base}(\mathbf{H_3PO_4})_n] - n \times E[\mathbf{H_3PO_4}] - E[\mathbf{base}]$ ). <sup>c</sup>Binding energy per PA molecule.

been transferred to the base molecule except in the complex of CRT\* + 1PA. Specifically, the smallest binding energy of the first PA molecule paired with IMI through the shortest hydrogen bond O···N1 results from the partial covalent bond between the proton and N1 of the IMI molecule; that is, the proton in closest proximity to IMI is shared by the proton donor oxygen and the proton acceptor nitrogen.

**Energetics of Proton Transfer.** The PES scans for proton transfer were performed with respect to the fully optimized structures. The relative energy profiles shown in Figures 3–5 are plotted as a function of the asymmetric stretch coordinate,  $q_{\rm asym} = 1/2(r_{\rm D\cdots H} - r_{\rm H\cdots A})$ , where D indicates the nitrogen or oxygen atom initially covalently bonded to the proton and A represents the nitrogen or oxygen atom acting as the proton

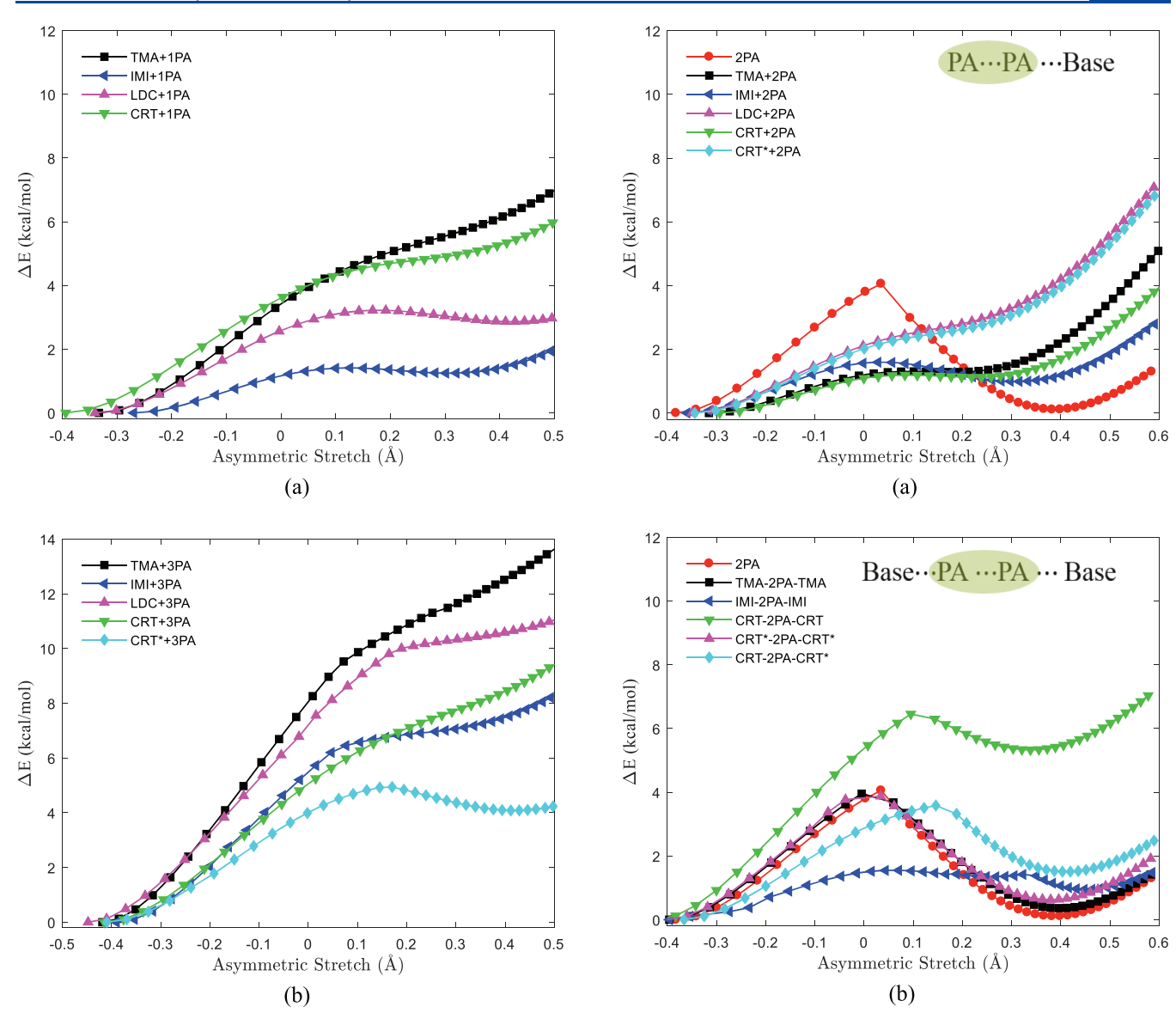


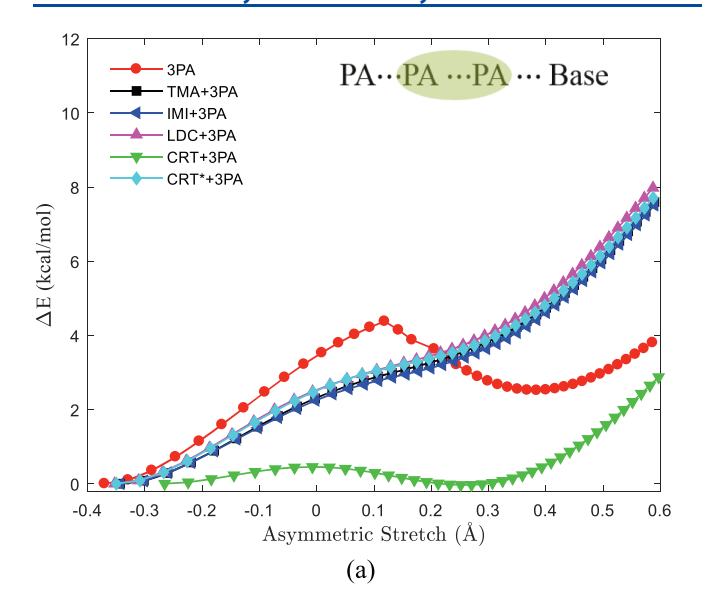
Figure 3. Energetics for proton transfer from protonated base to PA in systems of cluster of (a) one PA molecules with TMA, IMI, LDC, and CRT and (b) three PA molecules with TMA, IMI, LDC, and CRT at the B3LYP/6-311G\*\*/SMD level of theory. The energetics for transfer of a proton from protonated TMA or CRT to PA is monotonically increasing in both base + 1PA and base + 3PA systems, demonstrating that the ionic pairs are energetically preferable and stable in these systems. Although there is a relatively tiny second well in IMI + 1PA and LDC + 1PA systems, the second well would disappear as the number of PA molecules in the cluster increases.

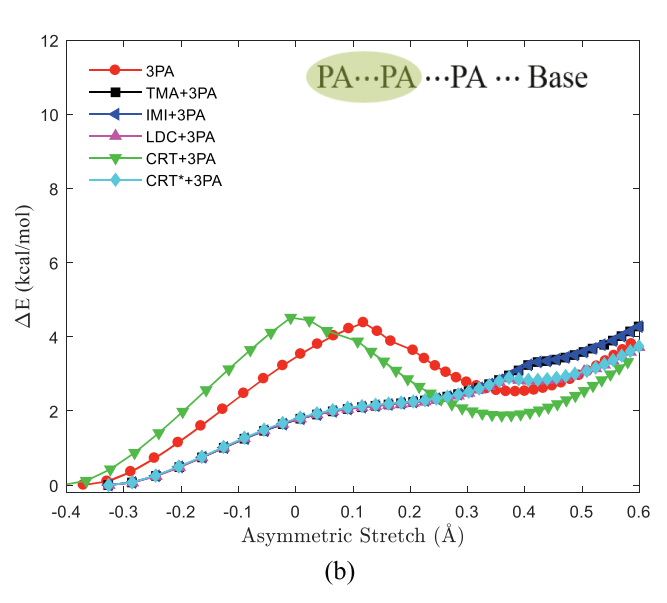
acceptor. As indicated previously, the PA molecule has dissociated one proton to the base in all systems excepting the CRT\* + 1PA complex. Thus, it is necessary to investigate the proton transfer from the base to PA molecule. The relative energy profiles for proton transfer from the protonated N1 atom of the base to the PA molecule through the hydrogen bond between them in systems of base + 1PA and base + 3PA were determined at the B3LYP/6-311G\*\* level of theory with the inclusion of the implicit SMD continuum solvation model, as shown in Figure 3. All curves demonstrate that the bridging proton between the PA and the base has a marked propensity of remaining associated with the base. In both systems of TMA + 1PA and CRT + 1PA shown in Figure 3a, the relative energy

Figure 4. Energetics for proton transfer between the PA molecules in systems of (a) cluster of two PA molecules with TMA, IMI, LDC, CRT, and CRT\* and (b) cluster of two PA subunits flanked by two base molecules at the B3LYP/6-311G\*\*/SMD level of theory. Note that the bases with stronger proton affinity exert greater influence on the energetics for proton transfer between individual PA molecules. However, the effects are minimal when the potentials are shifted into the single-well from the double-well. The double-well potential recovers with deformations in various manners when one additional base molecule is added to the other side of these complexes forming (base···PA···PA···base) clusters.

profiles reveal a monotonically increasing trend, indicating that there is only one minimum energy structure, that is the contact ion pair, base—H<sup>+</sup>····PA<sup>-</sup>, which attributes its stability to the effect of the implicit continuum solvation and the strong basicity of the base. There is a very shallow minimum in the clusters of LDC + 1PA and IMI + 1PA. This is because in the LDC + 1PA complex another hydrogen bond between the proton donor oxygen of the PA molecule and O1 atom of LDC stabilizes the charge distribution accompanying the proton transfer event, which can be confirmed by the contraction of the hydrogen bond O···O1 (from 2.77 to 2.61 Å) and the slight elongation of the O–H bond length (from 0.98 to 1.00

Article





**Figure 5.** Energetics for proton transfer between (a) first and second PA and (b) second and third PA in systems of cluster consisting of three PA molecules with TMA, IMI, LDC, CRT, and CRT\* at the B3LYP/6-311G\*\*/SMD level of theory. Note that the neighboring cation base—H+ results in either a negligible energetic barrier or a single minimum between the first and second PA molecules. The energetics for proton transfer in systems of base + 3PA (base = TMA, IMI, CRT\*, and LDC) have similar trends in which the energies are monotonically increasing without the formation of a TS. Barrierless proton transfer occurs in the system of CRT with several PA molecules.

Å). It is important to note that the second hydrogen bond in the CRT + 1PA pair strengthens the dissociation of the PA molecule because the N2 atom donates a hydrogen bond to PA, which causes higher endothermicity for proton transport in CRT + 1PA than LDC + 1PA. However, in the IMI + 1PA system, the lowest endothermicity for transferring of the proton results from the weakening covalent bond between the proton and the N1 atom of IMI. On the other hand, these small wells may disappear when the ZPE-corrected energies are included as the ground vibrational energy is probably higher than this tiny barrier.

Figure 3b illustrates the higher energetics for proton transfer from protonated base to the PA molecule upon the addition of three PA molecules to various bases in comparison to those shown in Figure 3a. This means that the extra PA molecules act to retain the proton on the bases. This observation is consistent with the AIMD results that there is no proton backtransfer from IMI-H+ to PA or PA- occurring in the PA/IMI (2:1) system. 41 It is interesting to note that the low energetics with a second well for proton transfer is observed in the congener of CRT\* + 3PA because there is proton transfer simultaneously occurring from the first PA to the second PA (see Figure S3) and the reorientation of the hydrogen bonding, while this phenomenon is not shown in the cluster of LDC + 3PA that possesses the analogous hydrogen bond network to the CRT\* + 3PA system. These differences may be caused in part by two different situations in proton affinity for LDC and CRT: one site of LDC with strong proton affinity and another site with considerably weak proton affinity (i.e., 290.15 kcal/ mol vs 264.11 kcal/mol); both sites of the CRT molecule have medium proton affinities (i.e. 286.04 kcal/mol vs 273.09 kcal/ mol), as reported in Table 1. Another crucial factor is the huge difference in the geometries of LDC and CRT. It may be concluded that the ionicity of these PILs is reasonably high based on these calculations.

Of particular interest is the influence of the protonated bases (i.e. base-H<sup>+</sup>) on the energetics for proton transfer from one PA molecule to another. The relative proton-transfer energy profiles for both clusters of (H<sub>3</sub>PO<sub>4</sub>)<sub>2</sub> and (H<sub>3</sub>PO<sub>4</sub>)<sub>3</sub> are illustrated with a red line as a reference for comparison in Figures 4 and 5. Compared with the energetics for proton transfer within PA clusters in the gas phase, "7 the trends are similar to each other, but the energetic barrier is almost equivalent for the (H<sub>3</sub>PO<sub>4</sub>)<sub>2</sub> cluster while much lower in the solvation SMD model than in the gas phase for the cluster of  $(H_3PO_4)_3$ . It should be pointed out that the proton transfer exactly occurs in the cluster of  $(H_3PO_4 \cdot H_2PO_4)^-$  or  $(H_3PO_4 \cdot H_3PO_4)^ H_3PO_4 \cdot H_2PO_4$  in the proximity of a positively charged base molecule instead of the pure PA clusters. To some extent, the cationic base-H<sup>+</sup> may be treated as a substituent hydrogen bonded to the PA molecules, but it is more complex because the bases have different proton affinities and possess various proton acceptor and/or donor sites.

The energetics for transferring a proton between two PA molecules in the systems with two added PA molecules are shown in Figure 4a. The curves indicate that the symmetric double-well potential for proton transfer are distorted to various extents, leading to a considerable weakening of the barriers with small secondary wells in the systems of base + 2PA (base = IMI, CRT, and TMA) and the single minimum potential in the complexes of base + 2PA (base = LDC and CRT\*). These changes may be ascribed to the different proton affinities of these bases: IMI < CRT < TMA < LDC (reported in Table 1). Although the proton affinity of a single site of CRT is somewhat smaller than TMA, the cooperative effects of the two proton acceptor sites rather than one acceptor and one donor strengthen the ability of attracting a proton. Interestingly, when the single-well potential appears, the differences are not discernible in comparison to the curves of LDC + 2PA and CRT\* + 2PA, which will be further borne out by examining the energetic profiles for proton transfer between PA molecules in the systems of base + 3PA (see below).

To aid in understanding the effects of the base molecules, one additional base molecule was added to the "other side" of

these complexes forming (base···PA···PA···base) clusters (base = TMA, IMI, CRT, and CRT\*) including (CRT···PA···PA··· CRT\*). Note that the LDC was not included due to the enormous computational cost. It is not surprising to observe that the double-well potential recovers with deformations in various degrees. First, the curves of the proton-transfer energetics coincide with the reference in the systems of (base···PA···PA···base) (base = TMA and CRT\*), which implies that the influence of the initial base molecule is exactly counterbalanced by the additional identical base. It should be noted that the energetic barrier is dramatically higher in the CRT···PA···PA···CRT system. This may be because the electron density of proton-accepting oxygen atoms of PA molecules is shared by the proton-donating N2 atoms, leading to the attenuation of attracting the proton. In addition, the symmetry was distorted upon adding the CRT to CRT\* + 2PA complex, consequently giving rise to a slight decrease in the energetic barrier to proton transfer with a less energetically favorable configuration after transferring the proton. The relatively small penalty for proton transfer occurs in the system (IMI···PA···PA···IMI) due to the feasible movement of the bridging proton between the base and the PA molecule to stabilize the system during the proton transfer. The adjustment of the bridging proton is due to the moderate proton affinity of

Figure 5 displays the energetics for transferring a proton between the first and second PA molecules as well as between the second and third PA molecules in the complexes of a base paired with three PA molecules. It is worthy of noting that the neighboring cation base-H+ results in either a negligible energetic barrier or a single minimum for the proton-transfer energetics between the first and second PA molecules, as shown in Figure 5a. More specifically, the monotonically increasing curves are nearly coincident with each other in the base + 3PA complexes (base = TMA, IMI, LDC, and CRT\*). The similarity in these systems is that the base is hydrogen bonded to a PA via only one proton accepting site or two proton accepting sites. It may be concluded that the involvement of only proton accepting sites of the base molecule could lead to the analogous energetic situation on the proton transfer between the central PA subunits flanked by a cation and a neutral PA molecule. The endothermicity for proton transfer is roughly 4 kcal/mol, a similar value to the barrier to transfer a proton in the cluster of (H<sub>3</sub>PO<sub>4</sub>)<sub>3</sub>, if the asymmetric stretch coordinate where the second well resides in the pure cluster of  $(H_3PO_4)_3$  are treated as the final (or end) position in the transfer. Nevertheless, the occurrence of a negligible barrier to proton transfer in the system of CRT + 3PA does not mean that the small barrier would appear as long as there is a proton-donating site of the base molecule involved in the neighboring hydrogen bonding networks. In terms of dynamics, the proton transfer in PA clusters could facilely happen when protonated base molecule approaches this cluster and forms such a hydrogen bonding network at the cost of 2 kcal/mol (the difference in energy between the second minimum and endothermicity). Again, the monotonically increasing curves (i.e., in the cases with a single-well potential) of the proton-transfer energetics between the second and third PA molecules in Figure 5b that nearly coincide indicate that the effects of the protonated bases are quite insensitive to the specific molecular geometries and the proton affinities except for the case in which the proton-donating site of the base molecule is involved. This pattern is further underscored by

comparing the results of the CRT + 3PA and CRT\* + 3PA systems in which the differences are the hydrogen bonds formed through different pairs of proton donor and acceptor sites. It is surprising to observe that the endothermicities decrease in comparison to the energetics for proton transfer between PA molecules in the vicinity of the cationic ions (shown in Figure 5a). The flattening of these curves may be the result of the better stabilization of charge by the neighboring PA molecule when in proximity to the bases. However, the curve of the proton-transfer energetics in the CRT + 3PA complex resembles that in a pure (or neat) PA cluster but shifts to the left with a lower well. The formation of a contact ion pair in CRT + 3PA may be responsible for the weakening influence of the base molecule on the energetics for proton transfer between the second and third PA molecules.

Assuming that the computed energetics in these small clusters reflect the behavior in the bulk systems and that the entropic effects would not qualitatively change the observed trends, we can speculate about the behavior of the proton transport in mixtures of PA with the bases. According to the analysis in the present study, the proton transferred from a PA molecule to any of the bases examined here remains with the base (i.e., protonating the base) and might not contribute significantly to the proton conductivity of the bulk system. At the same time, the presence of a protonated base and the existence of the deprotonated PA molecules polarize the network of the hydrogen-bonded PA molecules. As a result, the energy barrier for proton transfer between the neighboring PA molecules is decreased. Thus, changes of the proton conductivity in PA with specific bases might be caused by the changes in the energy barrier for the proton transfer between the PA molecules, rather than due to the proton transfer between the base and PA molecules. AIMD simulations on larger and extended systems should provide verification of this proposed idea.

## CONCLUSIONS

Ab initio molecular orbital calculations were performed to determine the fully optimized structures of TMA, IMI, LDC, and CRT with the addition of 1-3 PA molecules at the B3LYP/6-311G\*\* level with the inclusion of implicit solvation effects ( $\varepsilon = 61$ ). It was found that the proton dissociation from the PA molecule occurs in all systems, resulting in the formation of ion pairs of the protonated base and negatively charged anion H<sub>2</sub>PO<sub>4</sub><sup>-</sup> due to the relatively strong basicity of the bases and the effect of the high dielectric constant solvent on stabilizing the charge separation. The second and third PA molecules preferentially form "ring-like" hydrogen bonds ranging from 2.48 to 2.73 Å with a PA molecule rather than with available hydrogen bond donor and acceptor sites of the base. Examination of the ZPE-corrected binding energies of the PA molecules to various bases indicates that the first PA molecule is the most loosely bound to the IMI molecule in comparison with other systems. The binding energy per PA molecule increases with the addition of more PA molecules because the second and third PA molecules form double hydrogen bonds with a PA molecule. The strongest binding energy was observed in the CRT systems.

PES scans were carried out with respect to the optimized configurations to investigate the effects of the bases on the energetics for proton transfer between the PA molecules. It was found that the bases with stronger proton affinities exert greater influence on the energetics for proton transfer between

the PA molecules. However, the effects are minimal when the potentials are shifted into the single-well from the double-well. There is energetic barrierless proton transfer occurring in the system of CRT + 3PA, implying that the CRT may be a better potential candidate in the PA-based PILs. Although these static electronic structure calculations provide some guidelines in understanding proton transfer in PILs, it is crucial to consider additional factors including quantum nuclear effects, dynamic bond length fluctuations, and effects of the extended hydrogen bond network. Hence, AIMD simulations will be carried out on these systems in our future work.

## ASSOCIATED CONTENT

# Supporting Information

The Supporting Information is available free of charge at https://pubs.acs.org/doi/10.1021/acs.jpca.0c02863.

Energetics for proton transfer between first and second PA molecules in the system of CRT + 3PA with various dielectric constants at the B3LYP/6-311G\*\*/SMD level of theory; fully optimized configurations of cluster of two PA molecules with TMA, IMI, LDC, CRT, and CRT\*; and configurations of cluster CRT\* + 3PA shown correspond to the structure of the maximum and the structure of the second minimum during the proton transfer from N1 of CRT\* to PA (PDF)

## AUTHOR INFORMATION

## **Corresponding Author**

Stephen J. Paddison — Department of Chemical and Biomolecular Engineering, University of Tennessee, Knoxville, Tennessee 37996, United States; orcid.org/0000-0003-1064-8233; Email: spaddison@utk.edu; Fax: +1 865 974 2026

#### **Authors**

Zhenghao Zhu — Department of Chemical and Biomolecular Engineering, University of Tennessee, Knoxville, Tennessee 37996, United States

**Xubo Luo** — Department of Chemical and Biomolecular Engineering, University of Tennessee, Knoxville, Tennessee 37996, United States; ⊚ orcid.org/0000-0002-1591-7466

Alexei P. Sokolov — Department of Chemistry, University of Tennessee, Knoxville, Tennessee 37996; Chemical Sciences Division, Oak Ridge National Laboratory, Oak Ridge, Tennessee 37831, United States; orcid.org/0000-0002-8187-9445

Complete contact information is available at: https://pubs.acs.org/10.1021/acs.jpca.0c02863

### Notes

The authors declare no competing financial interest.

#### ACKNOWLEDGMENTS

This work was supported by the National Science Foundation under CHE 1764409: "Mechanisms of Proton Transport in Ionic Liquids: Grotthuss *versus* Vehicular". Computing resource was provided through an XSEDE allocation award: DMR130078.

### REFERENCES

- (1) Greaves, T. L.; Drummond, C. J. Protic Ionic Liquids: Evolving Structure-Property Relationships and Expanding Applications. *Chem. Rev.* **2015**, *115*, 11379–11448.
- (2) Wojnarowska, Z.; Grzybowska, K.; Hawelek, L.; Swiety-Pospiech, A.; Masiewicz, E.; Paluch, M.; Sawicki, W.; Chmielewska, A.; Bujak, P.; Markowski, J. Molecular Dynamics Studies on the Water Mixtures of Pharmaceutically Important Ionic Liquid Lidocaine HCl. *Mol. Pharm.* **2012**, *9*, 1250–1261.
- (3) Austen Angell, C.; Ansari, Y.; Zhao, Z. Ionic Liquids: Past, Present and Future. Faraday Discuss. 2012, 154, 9-27.
- (4) Adrjanowicz, K.; Kaminski, K.; Paluch, M.; Wlodarczyk, P.; Grzybowska, K.; Wojnarowska, Z.; Hawelek, L.; Sawicki, W.; Lepek, P.; Lunio, R. Dielectric Relaxation Studies and Dissolution Behavior of Amorphous Verapamil Hydrochloride. *J. Pharm. Sci.* **2010**, *99*, 828–839.
- (5) Wojnarowska, Z.; Paluch, K. J.; Shoifet, E.; Schick, C.; Tajber, L.; Knapik, J.; Wlodarczyk, P.; Grzybowska, K.; Hensel-Bielowka, S.; Verevkin, S. P.; et al. Molecular Origin of Enhanced Proton Conductivity in Anhydrous Ionic Systems. *J. Am. Chem. Soc.* **2015**, 137, 1157–1164.
- (6) Wojnarowska, Z.; Wang, Y.; Paluch, K. J.; Sokolov, A. P.; Paluch, M. Observation of Highly Decoupled Conductivity in Protic Ionic Conductors. *Phys. Chem. Chem. Phys.* **2014**, *16*, 9123–9127.
- (7) Mogurampelly, S.; Keith, J. R.; Ganesan, V. Mechanisms Underlying Ion Transport in Polymerized Ionic Liquids. *J. Am. Chem. Soc.* **2017**, *139*, 9511–9514.
- (8) Wang, C.; Clark, J. K., II; Kumar, M.; Paddison, S. J. An ab initio Study of the Primary Hydration and Proton Transfer of CF3SO3H and CF3O(CF2)2SO3H: Effects of the Hybrid Functional and Inclusion of Diffuse Functions. *Solid State Ionics* **2011**, 199-200, 6–13.
- (9) Tuckerman, M. E.; Chandra, A.; Marx, D. A Statistical Mechanical Theory of Proton Transport Kinetics in Hydrogen-Bonded Networks Based on Population Correlation Functions with Applications to Acids and Bases. *J. Chem. Phys.* **2010**, *133*, 124108.
- (10) Hayes, R. L.; Paddison, S. J.; Tuckerman, M. E. Proton Transport in Triflic Acid Hydrates Studied via Path Integral Car–Parrinello Molecular Dynamics. *J. Phys. Chem. B* **2009**, *113*, 16574–16589.
- (11) Elliott, J. A.; Paddison, S. J. Modelling of Morphology and Proton Transport in PFSA Membranes. *Phys. Chem. Chem. Phys.* **2007**, *9*, 2602–2618.
- (12) Greenwood, N. N.; Thompson, A. Proton-Switch as a Mechanism for Conduction in Anhydrous Phosphoric Acid. *Proc. Chem. Soc., London* **1958**, 352–353.
- (13) Suwannakham, P.; Chaiwongwattana, S.; Sagarik, K. Proton Dissociation and Transfer in Hydrated Phosphoric Acid Clusters. *Int. J. Quantum Chem.* **2015**, *115*, 486–501.
- (14) Clark, J. K., II; Paddison, S. J. Ab initio Molecular Dynamics Simulations of Water and an Excess Proton in Water Confined in Carbon nanotubes. *Phys. Chem. Chem. Phys.* **2014**, *16*, 17756.
- (15) Vilčiauskas, L.; Tuckerman, M. E.; Bester, G.; Paddison, S. J.; Kreuer, K. D. The Mechanism of Proton Conduction in Phosphoric Acid. *Nat. Chem.* **2012**, *4*, 461–466.
- (16) Habenicht, B. F.; Paddison, S. J. Ab initio Simulations of the Effects of Nanoscale Confinement on Proton Transfer in Hydrophobic Environments. *J. Phys. Chem. B* **2011**, *115*, 10826–10835.
- (17) Vilciauskas, L.; Paddison, S. J.; Kreuer, K.-D. Ab Initio Modeling of Proton Transfer in Phosphoric Acid Clusters. *J. Phys. Chem. A* **2009**, *113*, 9193–9201.
- (18) Li, S.; Qian, W.; Tao, F.-M. Ionic Dissociation of Methanesulfonic Acid in Small Water Clusters. *Chem. Phys. Lett.* **2007**, 438, 190–195.
- (19) Vuilleumier, R.; Borgis, D. Proton Conduction: Hopping Along Hydrogen Bonds. *Nat. Chem.* **2012**, *4*, 432–433.
- (20) Hoarfrost, M. L.; Tyagi, M.; Segalman, R. A.; Reimer, J. A. Proton Hopping and Long-Range Transport in the Protic Ionic Liquid [Im][TFSI], Probed by Pulsed-Field Gradient NMR and

- Quasi-Elastic Neutron Scattering. J. Phys. Chem. B 2012, 116, 8201–8209.
- (21) Kreuer, K. D.; Fuchs, A.; Ise, M.; Spaeth, M.; Maier, J. Imidazole and Pyrazole-based Proton Conducting Polymers and Liquids. *Electrochim. Acta* 1998, 43, 1281–1288.
- (22) Sepehr, F.; Paddison, S. J. Primary Hydration and Proton Transfer of Electrolyte Acids: An ab initio Study. *Solid State Ionics* **2017**, *306*, 2–12.
- (23) Sepehr, F.; Paddison, S. J. Effect of Sulfuric and Triflic Acids on the Hydration of Vanadium Cations: An ab Initio Study. *J. Phys. Chem. A* **2015**, *119*, 5749–5761.
- (24) Clark, J. K., II; Paddison, S. J. Side Chain Flexibility in Perfluorosulfonic Acid Ionomers: an ab initio Study. *J. Phys. Chem. A* **2013**, *117*, 10534–10543.
- (25) Clark, J. K., II; Paddison, S. J.; Hamrock, S. J. The Effect of Hydrogen Bond Reorganization and Equivalent Weight on Proton Transfer in 3M Perfluorosulfonic Acid Ionomers. *Phys. Chem. Chem. Phys.* **2012**, *14*, 16349–16359.
- (26) Clark, J. K., II; Paddison, S. J.; Eikerling, M.; Dupuis, M.; Zawodzinski, T. A. A Comparative Ab Initio Study of the Primary Hydration and Proton Dissociation of Various Imide and Sulfonic Acid Ionomers. *J. Phys. Chem. A* **2012**, *116*, 1801–1813.
- (27) Feng, S.; Voth, G. A. Proton Solvation and Transport in Hydrated Nafion. J. Phys. Chem. B 2011, 115, 5903-5912.
- (28) Paddison, S. J.; Kreuer, K.-D.; Maier, J. About the Choice of the Protogenic Group in Polymer Electrolyte Membranes: Ab initio Modelling of Sulfonic Acid, Phosphonic Acid, and Imidazole Functionalized Alkanes. *Phys. Chem. Chem. Phys.* **2006**, *8*, 4530–4542.
- (29) Escribano, R.; Couceiro, M.; Gómez, P. C.; Carrasco, E.; Moreno, M. A.; Herrero, V. J. The Nitric Acid Hydrates: Ab Initio Molecular Study, and RAIR Spectra of the Solids. *J. Phys. Chem. A* **2003**, *107*, 651–661.
- (30) Scheiner, S.; Yi, M. Proton Transfer Properties of Imidazole. *J. Phys. Chem.* **1996**, *100*, 9235–9241.
- (31) Scheiner, S. Bent Hydrogen Bonds and Proton Transfers. Acc. Chem. Res. 1994, 27, 402–408.
- (32) Scheiner, S. Theoretical Studies of Proton Transfers. Acc. Chem. Res. 1985, 18, 174–180.
- (33) Scheiner, S. Proton Transfers in Hydrogen-bonded Systems. 4. Cationic Dimers of Ammonia and OH2. *J. Phys. Chem.* **1982**, *86*, 376–382.
- (34) Scheiner, S. Comparison of Proton Transfers in Teterodimers and Homodimers of NH3 and OH2. *J. Chem. Phys.* **1982**, *77*, 4039–4050.
- (35) Scheiner, S.; Harding, L. B. Proton Transfers in Hydrogenbonded Systems. 2. Electron Correlation Effects in Diamminehydrogen(1+). J. Am. Chem. Soc. 1981, 103, 2169-2173.
- (36) Scheiner, S. Proton Transfers in Hydrogen-bonded Systems. Cationic Oligomers of Water. *J. Am. Chem. Soc.* **1981**, *103*, 315–320.
- (37) Wang, C.; Paddison, S. J. Proton Transfer in Functionalized Phosphonic Acid Molecules. *Phys. Chem. Chem. Phys.* **2010**, *12*, 970–981.
- (38) Kumar, M.; Venkatnathan, A. Mechanism of Proton Transport in Ionic-Liquid-Doped Perfluorosulfonic Acid Membranes. *J. Phys. Chem. B* **2013**, *117*, 14449–14456.
- (39) Pant, R.; Kumar, M.; Venkatnathan, A. Quantum Mechanical Investigation of Proton Transport in Imidazolium Methanesulfonate Ionic liquid. *J. Phys. Chem. C* **2017**, *121*, 7069–7080.
- (40) Kumar, M.; Venkatnathan, A. Quantum Chemistry Study of Proton Transport in Imidazole Chains. *J. Phys. Chem. B* **2015**, *119*, 3213–3222.
- (41) Vilčiauskas, L.; Tuckerman, M. E.; Melchior, J. P.; Bester, G.; Kreuer, K.-D. First Principles Molecular Dynamics Study of Proton Dynamics and Transport in Phosphoric Acid/Imidazole (2:1) System. *Solid State Ionics* **2013**, *252*, 34–39.
- (42) Frisch, M. J.; Trucks, G. W.; Schlegel, H. B.; Scuseria, G. E.; Robb, M. A.; Cheeseman, J. R.; Scalmani, G.; Barone, V.; Mennucci, B.; Petersson, G. A.; et al. *Gaussian 09*, Revision E.01; Gaussian, Inc.: Wallingford, CT, 2013.

- (43) Becke, A. D. A New Mixing of Hartree-Fock and Local Density-Functional Theories. *J. Chem. Phys.* **1993**, 98, 1372–1377.
- (44) Hariharan, P. C.; Pople, J. A. The Influence of Polarization Functions on Molecular Orbital Hydrogenation Energies. *Theor. Chim. Acta* 1973, 28, 213–222.
- (45) Schlegel, H. B. Optimization of Equilibrium Geometries and Transition Structures. *J. Comput. Chem.* **1982**, *3*, 214–218.
- (46) Becke, A. D. Density-functional Thermochemistry. III. The Role of Exact Exchange. J. Chem. Phys. 1993, 98, 5648-5652.
- (47) Becke, A. D. Density-functional Thermochemistry. II. The Effect of the Perdew-Wang Generalized-gradient Correlation Correction. *J. Chem. Phys.* **1992**, *97*, 9173–9177.
- (48) Becke, A. D. Density-functional Thermochemistry. I. The Effect of the Exchange-only Gradient Correction. *J. Chem. Phys.* **1992**, *96*, 2155–2160.
- (49) Lee, C.; Yang, W.; Parr, R. G. Development of the Colle-Salvetti Correlation-energy Formula into a Functional of the Electron Density. *Phys. Rev. B* **1988**, *37*, 785–789.
- (50) McLean, A. D.; Chandler, G. S. Contracted Gaussian Basis Sets for Molecular Calculations. I. Second Row Atoms, Z= 11–18. *J. Chem. Phys.* **1980**, 72, 5639–5648.
- (51) Grimme, S. Semiempirical GGA-type Density Functional Constructed with a Long-range Dispersion Correction. *J. Comput. Chem.* **2006**, 27, 1787–1799.
- (52) Marenich, A. V.; Cramer, C. J.; Truhlar, D. G. Universal Solvation Model Based on Solute Electron Density and on A Continuum Model of the Solvent Defined by the Bulk Dielectric Constant and Atomic Surface Tensions. *J. Phys. Chem. B* **2009**, *113*, 6378–6396.
- (53) Munson, R. A. Dielectric Constant of Phosphoric Acid. *J. Chem. Phys.* **1964**, *40*, 2044–2046.
- (\$4) Sepehr, F.; Paddison, S. J. The Solvation Structure and Thermodynamics of Aqueous Vanadium Cations. *Chem. Phys. Lett.* **2013**, 585, 53–58.
- (55) Krakowiak, J.; Lundberg, D.; Persson, I. A Coordination Chemistry Study of Hydrated and Solvated Cationic Vanadium Ions in Oxidation States +III, +IV, and +V in Solution and Solid State. *Inorg. Chem.* **2012**, *51*, 9598–9609.
- (56) Li, X.; Frisch, M. J. Energy-represented Direct Inversion in the Iterative Subspace within a Hybrid Geometry Optimization Method. *J. Chem. Theory Comput.* **2006**, *2*, 835–839.
- (57) Hunter, E. P. L.; Lias, S. G. Evaluated Gas Phase Basicities and Proton Affinities of Molecules: An Update. *J. Phys. Chem. Ref. Data* **1998**, *27*, 413–656.